

NASA CR-178,16

NASA Contractor Report 178167 •

ICASE REPORT NO. 86-49

NASA-CR-178167
19860023203

ICASE

A NUMERICAL STUDY OF SEPARATION ON A
SPHEROID AT INCIDENCE

M. Rosenfeld
M. Israeli
M. Wolfshtein

LIBRARY COPY

OCT 8 1986

Contract Nos. NAS1-17070, NAS1-18107
July 1986

LANGLEY RESEARCH CENTER
LIBRARY, NASA
HAMPTON, VIRGINIA

INSTITUTE FOR COMPUTER APPLICATIONS IN SCIENCE AND ENGINEERING
NASA Langley Research Center, Hampton, Virginia 23665

Operated by the Universities Space Research Association



National Aeronautics and
Space Administration

Langley Research Center
Hampton, Virginia 23665



NF00194

A NUMERICAL STUDY OF SEPARATION ON A SPHEROID AT INCIDENCE

M. Rosenfeld^{*}, M. Israeli⁺, and M. Wolfshtein⁼

Technion - Israel Institute of Technology

Haifa, Israel

ABSTRACT

The three-dimensional incompressible, steady and laminar flow field around a prolate spheroid at incidence is considered. The parabolized Navier-Stokes equations are solved numerically. The method can handle vortex type as well as bubble type flow separation because the pressure is one of the dependent variables. In the present paper the distribution of the skin friction is reported for two test cases. The first test case is a prolate spheroid of aspect ratio of 4:1 at 6° incidence and Reynolds number of 10^6 (based on half the major axis). The second case is a spheroid with a 6:1 aspect ratio at 10° incidence and Reynolds number of $0.8 \cdot 10^6$. The properties of the flow field near the body are discussed on the basis of the pattern of the skin friction lines, and the shape of the separation lines. Favorable agreement with experimental results is obtained.

The research for the second author was supported under the National Aeronautics and Space Administration under NASA Contract Nos. NAS1-17070 and NAS1-18107 while in residence at the Institute for Computer Applications in Science and Engineering (ICASE), NASA Langley Research Center, Hampton, VA 23665.

^{*}Graduate Instructor, Department of Aeronautical Engineering. Member AIAA.

⁺Professor, Department of Computer Sciences. Member AIAA.

⁼Associate Professor, Department of Aeronautical Engineering. Member AIAA.

Introduction

The analysis of incompressible three-dimensional flows around slender bodies at incidence is very important in modern aerodynamics and hydrodynamics. The flow field is characterized by crossflow reversal, localized thickening of the boundary layer, formation of longitudinal vortices, regions of backward flow and strong viscous-inviscid interaction¹. The complicated phenomenon of flow separation is of special importance to aerodynamic designers as it has a major influence on the aerodynamic coefficients. In two-dimensional flows the point of separation from a surface coincides with the point at which the wall shear stress vanishes. In three-dimensional flows, such a criterion does not exist. Indeed, the shear stress does not vanish on the separation line except, possibly, at isolated points. At present, the understanding of the three-dimensional flow separation relies mainly on observations drawn from the analysis of the flow pattern near the body. Particularly fruitful results were obtained by visualization of the pattern of the skin friction lines on the surface of wind tunnel models with oil streak techniques². The theory of the skin friction lines is based on Lighthill's work³ which shows that the skin friction lines have to obey certain topological rules. It is widely accepted now that a necessary condition for flow separation in three-dimensional flow fields is the convergence of many skin friction lines into a single line¹. Whether it is also a sufficient condition is a matter of current debate. In a similar manner, the divergence of the skin friction lines from a single line characterizes the attachment or reattachment of the flow.

We have already mentioned the difference between the nature of separation in two-dimensional and three-dimensional flows. This has given rise to various definitions of separation. Thus Maskel⁴ used experimental evidence

to classify two types of flow separation in three-dimensional flow fields: bubble type separation and free vortex type separation. In the bubble type separation the main direction of the flow is reversed in the separated zone. In the vortex type separation no velocity reversal occurs in the streamwise direction. The flow leaves an oblique separation line, usually as a free shear layer, and rolls up along the downstream direction. Thus only circumferentially reversed flow exists. Wang⁵ defines two kinds of flow separations as well, namely "closed" separation and "open" separation. These terms are based on the shape of the separation line. The closed and open separations are very similar to Maskel's bubble and vortex type separations, respectively. Other investigators prefer to describe the bubble type separation as "two-dimensional" separation, indicating the reversal of the mainstream direction, which is typical of separated regions of two-dimensional flow fields. The vortex type separation is called "three-dimensional" separation to emphasize the fact that this kind of flow separation may occur only in three-dimensional flow fields.

As the phenomenon considered is so complicated much of the research was restricted to simple geometries. One of the simplest possible geometries is the prolate spheroid, which has been studied experimentally⁶⁻⁷ and numerically⁸⁻¹⁵. In all the numerical calculations the boundary layer approximation was used. For instance, Wang⁸ solved the degenerate case of the boundary layer equations at the windward and at the leeward symmetry planes. Later, Wang⁹ computed the flow field around a spheroid of major to minor axis ratio of 4:1 at 6° incidence. A solution was obtained over a significant part of the body. At the rear part of the spheroid no solution could be found because of numerical instabilities. Wang concluded that the flow is separated there. Cebeci et al.¹⁰ obtained very similar results for

the same case and calculated the flow at other angles of attack as well. In the above computations, the boundary layer equations were solved by marching along both the axial and circumferential directions, but Hirsch and Cebeci¹¹ and Patel and Choi¹² solved the momentum equations by an ADI method which was expected to be more stable in circumferentially reversed flow regions. In addition, Hirsch and Cebeci¹¹ also solved what they call the "Parabolic-Elliptic Boundary Layer" equations in which the pressure field is known, but the circumferential diffusion terms are retained. No significant change in the results was reported.

The boundary layer equations for a 6:1 spheroid at incidence were solved by Schoenauer¹³ and Patel and Baek¹⁴. The code written by Schoenauer¹³ is for general bodies and uses adaptive high order methods with control on the truncation error bounds. Unfortunately, no detailed results which can be easily compared with other results are given. Stock¹⁵ solved the integral boundary layers equations for a variety of cases. Not surprisingly, reasonable agreement with the experiment was obtained only for those regions of the flow field in which the flow direction does not deviate significantly from that of the main flow.

In all the above mentioned boundary layer calculations flow fields without flow reversal were readily calculated. These methods may (with special treatment) handle also weak circumferential flow reversal, provided that separation does not occur. They can not handle separated flow of both kinds. In general the boundary layer approximation depends on specification of pressure, say by a potential flow solution. In such calculations the separation line cannot be reached, and the formation of numerical difficulties is usually interpreted as the onset of separation. Against this background we have to note the success of the thin layer approximation¹⁶ in the calculation of compressible separated flow on slender bodies at incidence. This is attributed to the fact that the pressure is not prescribed.

A solution of the full Navier-Stokes equations is very expensive and has been attempted only by few investigators. Haase¹⁷ solved the full equations using vorticity/velocity formulation, and a cartesian coordinate system. As the coordinates were not body-fitted special techniques were used near the wall. His results appear to suffer from too low a resolution, and we believe that his technique requires the addition of a potential velocity correction to ensure mass conservation.

In this paper, the laminar, steady and incompressible flow field around a prolate spheroid at incidence is investigated using numerical solutions of the parabolized Navier-Stokes equations in which the pressure is not predetermined. Consequently, the equations are not singular at separation lines and separated flow regions may be included in the solution domain. In the present work we consider the skin friction distribution only. The pattern of the skin friction lines is computed and particular attention is given to the separation lines.

Mathematical Model and Numerical Solution

The flow is approximated by the steady and incompressible Parabolized Navier-Stokes (PNS) equations which are obtained from the full Navier-Stokes equations by neglecting the streamwise diffusion terms in the momentum equations. This stands in contrast to the parabolic approximations to the Navier-Stokes equations (or the boundary layer equations) in which the pressure is given a priori. As the pressure is not predetermined in the parabolized Navier-Stokes equations the problem of singularity near separation (which is typical to the boundary layer equations) does not arise here.

The governing equations are formulated in a general axisymmetric curvilinear orthogonal coordinate system, using primitive variables, and

contravariant velocity components. The three coordinates ρ, θ, ξ (see Fig. 1) run in the normal, circumferential and the main stream direction, approximately. These coordinates are stretched to q, s, t coordinates respectively which are orthogonal as well. The equations are simplified neglecting the stream-wise diffusion terms. The equations are:

the continuity equation:

$$\frac{\partial(\sigma u)}{\partial q} + \frac{\partial(\tau v)}{\partial s} + \frac{\partial(\delta w)}{\partial t} = 0 \quad (1a)$$

the momentum equations:

q-component:

$$\begin{aligned} \frac{1}{h_q} M\left(\frac{u}{h_q}\right) + \frac{1}{2} \sigma \frac{\partial \beta}{\partial q} v^2 + \frac{1}{2} \sigma \frac{\partial \gamma}{\partial q} w^2 - \frac{1}{2} \delta \frac{\partial \alpha}{\partial t} uv = - \sigma \frac{\partial p}{\partial q} + \\ + \frac{1}{Re} \left\{ \frac{\partial}{\partial q} \left[\alpha \frac{\partial(\sigma u)}{\partial q} \right] + \frac{1}{\delta} \frac{\partial^2 u}{\partial s^2} + \frac{\partial}{\partial q} \left(\frac{1}{\delta} \right) \frac{\partial v}{\partial s} - \frac{\partial}{\partial q} \left(\delta \frac{\partial \alpha}{\partial t} w \right) \right\} \end{aligned} \quad (1b)$$

s-component:

$$\begin{aligned} \frac{1}{h_s} M\left(\frac{v}{h_s}\right) - \frac{1}{2} \delta \frac{\partial \beta}{\partial t} vw - \frac{1}{2} \sigma \frac{\partial \beta}{\partial q} uv = - \tau \frac{\partial p}{\partial s} + \\ + \frac{1}{Re} \left[\tau \beta \frac{\partial^2 v}{\partial s^2} + \frac{\partial}{\partial q} \left(\frac{1}{\delta} \frac{\partial v}{\partial q} \right) - \delta \frac{\partial \beta}{\partial t} \frac{\partial w}{\partial s} - \sigma \frac{\partial \beta}{\partial q} \frac{\partial u}{\partial s} \right] \end{aligned} \quad (1c)$$

t-component

$$\begin{aligned} \frac{1}{h_t} M\left(\frac{w}{h_t}\right) + \frac{1}{2} \delta \frac{\partial \beta}{\partial t} v^2 + \frac{1}{2} \delta \frac{\partial \alpha}{\partial t} u^2 - \frac{1}{2} \sigma \frac{\partial \gamma}{\partial q} uv = - \delta \frac{\partial p}{\partial t} + \\ + \frac{1}{Re} \left\{ \frac{\partial}{\partial q} \left(\frac{1}{\tau} \frac{\partial w}{\partial q} \right) + \frac{1}{\sigma} \frac{\partial^2 w}{\partial s^2} + \frac{\partial}{\partial q} \left[\frac{\partial}{\partial t} \left(\frac{1}{\tau} \right) u \right] + \frac{\partial}{\partial t} \left(\frac{1}{\sigma} \right) \frac{\partial v}{\partial s} \right\} \end{aligned} \quad (1d)$$

where

$$M = \sigma u \frac{\partial}{\partial q} + \tau v \frac{\partial}{\partial s} + \delta w \frac{\partial}{\partial t} \quad (2a)$$

$$\alpha = \frac{1}{h_q^2} \quad \sigma = \alpha J \quad (2b)$$

$$\beta = \frac{1}{h_s^2} \quad \tau = \beta J \quad (2c)$$

$$\gamma = \frac{1}{h_t^2} \quad \delta = \gamma J \quad (2d)$$

and J is the Jacobian:

$$J = h_q h_s h_t \quad (2e)$$

The Lamme coefficients are given by:

$$h_q^2 = \sum_{i=1}^3 \left(\frac{\partial X_i}{\partial q} \right)^2 \quad (3a)$$

$$h_s^2 = \sum_{i=1}^3 \left(\frac{\partial X_i}{\partial s} \right)^2 \quad (3b)$$

$$h_t^2 = \sum_{i=1}^3 \left(\frac{\partial X_i}{\partial t} \right)^2 \quad (3c)$$

where (X_1, X_2, X_3) is the cartesian coordinate system.

The contravariant velocity components V_q, V_s, V_t were transformed to:

$$u = h_q V_q \quad (4a)$$

$$v = h_s V_s \quad (4b)$$

$$w = h_t V_t \quad (4c)$$

In the present study, a prolate spheroidal coordinate system was chosen with the following Lamme coefficients:

$$h_q = a \frac{d\rho(q)}{dq} \operatorname{sh}^2 \rho(q) + \sin^2 \xi(t) \quad (5a)$$

$$h_s = a \frac{d\theta(s)}{ds} \operatorname{sh} \rho(q) \sin \xi(t) \quad (5b)$$

$$h_t = a \frac{d\xi(t)}{dt} \operatorname{sh}^2 \rho(q) + \sin^2 \xi(t) \quad (5c)$$

$\rho(q)$, $\theta(s)$, $\xi(t)$ are one-dimensional stretching functions.

The computed flow field did not cover the entire prolate spheroid. The upstream boundary was placed some distance downstream of the forward stagnation point at a region where the boundary layer approximation can still be justified and can provide the upstream boundary conditions for the PNS equations:

$$u = u_{up}, \quad v = v_{up}, \quad w = w_{up} \quad (6a)$$

where the subscript "up" stands for upstream conditions.

The downstream boundary was placed ahead of the rear stagnation point in order to minimize the usage of computational resources. It should be emphasized that the PNS equations are not singular at reversed flow regions, yet the bubble type separation at the rear part can be accurately computed only if the downstream boundary is moved far enough into the wake. Moreover, the calculation in the separated region was found to increase the number of iterations. Thus the total demand of computer resources became higher than our computer (IBM 3081D) could cope with. Due to the parabolization it is necessary to specify only one condition at the downstream boundary. We chose to specify a pressure boundary condition as follows:

$$\frac{\partial p}{\partial t} = \left(\frac{\partial p}{\partial t} \right)_{pot} \quad (6b)$$

where "pot" stands for the potential value.

The outer boundary was placed in the potential flow region. Three boundary conditions must be specified there, for example:

$$v = v_{\text{pot}}, \quad w = w_{\text{pot}}, \quad p = p_{\text{pot}} \quad (6c)$$

On the body the usual no-slip and no injection conditions were applied:

$$u = v = w = 0 \quad (6d)$$

Because of the symmetry of the flow, the solution was obtained for a half of the field only. On the leeward and windward symmetry planes symmetry conditions were used.

The finite difference equations written over a staggered grid were solved iteratively by a consistent and stable procedure without any further approximations. More details on the numerical method were reported by Rosenfeld and Israeli¹⁸ for the two-dimensional case and by Rosenfeld¹⁹ for the three-dimensional case.

A typical grid consisted of about 15000-20000 points: 25 in the normal and circumferential direction and 25 to 33 points along the spheroid. About one to two hours of CPU time were needed for a solution on an IBM 3081D computer, depending on the number of grid points and on the angle of attack. No standard convergence tests could be performed by systematically increasing the number of grid points because of the excessive computational cost. Nevertheless, some partial accuracy tests were conducted by varying the location of the outer and downstream boundaries while keeping the total number of mesh points constant. No significant differences were recorded for the cases reported in this paper.

Results

The flow field was solved about two slender prolate spheroids of major to minor axes ratio of 4:1 and 6:1 and for several angles of attack. For the sake of brevity, the results of only two cases will be reported here, one for each thickness ratio. All the calculations are for laminar flow. The Reynolds numbers chosen are such that laminar flow may be expected to prevail over much of the flow field (except at separated zones). In the presentation the streamwise coordinate is the normalized axial distance along the spheroid z (see Fig. 1): $z=-1$ and $z=1$ correspond to the nose and to the rear end of the spheroid respectively. The angles $\theta=0^\circ$ and $\theta=180^\circ$ correspond to the windward and leeward symmetry planes respectively.

3.1 A 4:1 spheroid at 6° incidence

Several numerical solutions of this case using the boundary layer equations were reported in the literature^{8-12,15}. Unfortunately, no experimental results are available for comparison with the calculations. Yet, comparison with previous boundary layer solutions is useful because at such a low incidence, the extent of the separated regions is very limited and therefore the boundary layer solutions may be expected to be quite similar to the parabolized Navier-Stokes results over a significant part of the spheroid. The Reynolds number based on half the length of the major axis of the spheroid and on the uniform velocity upstream of the body was set to 10^6 . The upstream boundary was placed at $z=-0.8$ and the initial conditions were approximated from the boundary layer solution of Wang⁸ for the same case.

The distributions of the skin friction coefficients are compared to the boundary layer approximation results of Wang⁸ and Patel and Choi¹² in

Figs. 2 and 3. The skin friction is normalized by the Reynolds number:

$$C_F = \frac{\tau_w}{\frac{1}{2}\rho U^2} \sqrt{Re} \quad (7)$$

where Re is the Reynolds number and τ_w is the shear stress on the wall, ρ is the density and U is the free stream velocity. Figures 2a and 2b show the distributions of the skin friction coefficient on the windward and leeward symmetry planes, respectively. Examination of the results show that the two boundary layer solutions are not identical. The difference between the two boundary layer solutions in both the windward and the initial part of the leeward side is fairly uniform. Our results lie generally between the two boundary layer solutions, although we used Wang's solution as the initial condition. However, in the downstream part of the leeward side the two boundary layer solutions approach one another, whereas the present value of the skin friction is somewhat higher. This region is characterized by the thickening of the boundary layer and ultimately separation occurs. The interaction between the separated flow and the pressure field is expected to lead to quite substantial departures from the potential pressure field specified in the boundary layer calculations, and consequently the disagreement between the present and boundary-layer results might have been expected.

In the present work, the separation point in the leeward plane is found to be at $z=0.75$ (see Fig. 2b). The separation points computed by the boundary layer approximation are quite close to one another: $z=0.724$, $z=0.72$ and $z=0.73$ for Wang⁸, Cebeci et al.¹⁰ and Patel and Choi¹² respectively. Once more, the difference may be attributed to the viscous-inviscid interaction which is neglected in the boundary layer approximation.

The circumferential distribution of the t and s components of the skin friction coefficient are shown in Fig. 3 at three axial locations, and compared with the data of Patel and Choi¹². As the agreement of the present skin friction coefficient on the planes of symmetry with Patel and Choi is not very good (see Fig. 2) it is not surprising that the present axial component of the skin friction in the frontal parts of the spheroid differs from the boundary layer one by a fairly uniform value. Another source for the disagreement can be found in the coarse circumferential resolution used by Patel and Choi: intervals of 20° in contrast to 7.5° in the present calculation. Still the circumferential component of the skin friction is in good agreement. The situation is different in the rear part of the spheroid where circumferentially reversed flow prevails and axial separation appears to be imminent.

The distribution of the calculated skin friction coefficient vectors on the unwrapped surface of the spheroid is shown in Fig. 4. Three distinct regions can be observed. In the first region, the vectors point towards the back and the leeward side of the spheroid. Further downstream and on the leeward side the direction of the vectors are shifted towards the windward side, suggesting the onset of a vortex. At the very end of the spheroid, the vectors point towards the nose, indicating the formation of a separation bubble. The solid line marks the location where the circumferential component of the shear stress reverses its direction.

The skin friction lines are tangent to the shear stress vector on the surface and can be computed¹ from:

$$\frac{h_s ds}{h_t dt} = \frac{C_{F,s}}{C_{F,t}} \quad (8)$$

As the skin friction lines are the projections of the streak lines near the body¹, their pattern may be instructive of the flow field in the vicinity of the body. Lighthill³ has shown that in the three-dimensional case the flow may separate from a solid body because of two reasons: $C_F \rightarrow 0$ and/or the convergence of the skin friction lines into one particular line. An attachment (or reattachment) line of the flow is characterized by the divergence of the skin friction lines away from the attachment line.

The skin friction lines were computed in the present work by solving (8) with a second order Runge-Kutta method. The components of the skin friction are interpolated using a bilinear spline approximation. The skin friction lines for the 4:1 spheroid at 6° incidence are shown in Figs. 5. Figure 5a shows the pattern on the unwrapped spheroid while the side, bottom and upper views of the skin friction lines on the spheroid are shown in Fig. 5b. Two types of skin friction lines convergence are evident: a very short swept line and a second line that appears to encircle the spheroid at about $z=0.70$. The second line of convergence is obviously a separation line that divides the flow into two regions: a region that is accessible to the flow from the forward stagnation point and a region that is not accessible and is in fact a bubble type separated region with reversed flow. In the terms of Wang⁹ this separation is called "closed" as it originates from a closed separation line. Figure 6 compares the zero circumferential shear stress line and the closed separation line with the results of Wang⁹ and Cebeci et al.¹⁰. The qualitative shape of the closed separation line is similar to other computations although the "tounge" of the separation line in our results is less pronounced and more close to the windward side. It should be noted that all separation phenomena are not likely to be well predicted by the boundary layer approximation. The agreement of the zero circumferential shear stress

line is much better, indicating that the boundary layer approximation is valid in regions not close to flow separation. Although there is circumferential flow reversal from about $z=-0.1$, the skin friction lines converge only at $z=0.45$ about 15° further in the leeward direction to the zero circumferential shear stress line (see Figs. 5a). However, the pattern of the skin friction lines is not sufficient to conclude whether a vortex type separation has occurred there.

The topology of the skin friction lines found in our calculations is notably similar to that conceived by Han and Patel⁶ from their flow field visualizations at 10° incidence and Reynolds number of $4 \cdot 10^4$ (see Fig. 10 in their paper). Cebeci et al.¹⁰ suggest three possibilities of the shape of the swept convergence line near the closed separation line. The present results are similar to their second option (Fig. 10 in their paper).

3.2 A 6:1 spheroid at 10° incidence

In this higher incidence case a bubble type separation exists as well as a free-vortex type separation. Some boundary layer solutions were reported for this case¹³⁻¹⁵. The experimental data available is reported by Kreplin et al.⁷ who measured the skin friction shear stress on a 6:1 spheroid at a Reynolds number of $8 \cdot 10^5$. The same Reynolds number was used in the present calculations.

The absolute magnitude of the normalized shear stress in several z stations is compared in Fig. 7 to the experimental values⁷ and to the computed boundary layer results of Patel and Baek¹⁴. The agreement at small distances from the upstream boundary is not good, possibly due to poor specification of the initial conditions at the upstream boundary in the present calculations which were approximated from Stock's integral boundary layer solution¹⁵. Further downstream the agreement of our calculation with

the experimental results improves while the results of Han and Baek get worse. Kreplin et al. related the high values of the skin friction near the leeward side to the transition of the separated flow to turbulent flow. In our laminar calculation this phenomenon cannot be reproduced.

Figure 8 shows the shear stress vector plot on the unwrapped spheroid. A minimum along the circumferential direction in the shear stress is clearly seen. It is interesting to note that due to three dimensional effects, this minimum does not occur along the leeward side where the potential adverse pressure gradient is maximal. Figure 9a shows the shear stress vector plot interpolated from our computations with the experimental results of Kreplin et al.⁷. In the laminar region of the flow field the agreement is usually good bearing in mind the complexity of the flow field and the difficulties in measuring the stress in the laminar regions as reported by Kreplin et al. However, the agreement at the initial stations near the leeward side is not as good. This is attributed to the poor initial conditions used in the present calculation at the upstream boundary. Figure 9b shows the same comparison with the boundary layer results of Schoenauer¹³. Boundary layer solutions were not obtained for significant parts of the flow field, although these are the most interesting regions where separation may occur. In the other regions, the agreement with our results is better than with the experimental results.

Figures 10 show the skin friction lines on the surface. In this case no bubble type separation is found in the region solved. On the other hand, a long and swept convergence line is present. The precise origin of the line cannot be defined with certainty. The skin friction lines merge into a line of convergence from both sides. It is interesting to note that now the zero circumferential shear stress line is only a small distance in the windward

direction from the convergence line. Again, it is impossible to predict the onset of an open type separation based on the properties of the flow field in the vicinity of the surface.

Kreplin et al. obtained the skin friction lines from the measured distribution of the shear stresses (Fig. 5 in [7]). The main separation line appears to be placed further in the leeward direction than the line we have computed. The differences may be explained by the transition to turbulent flow that occurred in the experiment, as turbulent flow can withstand higher adverse circumferential pressure drop before separation. Kreplin et al.⁷ observed a second separation line very close to the leeward side. We have not found this line, although there is a tendency of creating a second convergence line in the rear part of the spheroid.

Conclusions

The incompressible, steady and laminar parabolized Navier-Stokes equations were used to simulate the flow field around a prolate spheroid. Solutions were obtained not only in regions of attached flow, but also in domains where the flow is separated in the lateral and/or the axial direction. In this paper we concentrate only on the skin friction on the surface of the spheroid. Even so, this information is useful as it gives clues on the nature of the flow, and allows comparisons with available experimental and numerical data (anyhow, much of this data is confined to the skin friction). The results obtained agree with previous experimental data and numerical solutions of the boundary layer approximation, in the non-separated regions. In the separated region the skin friction is too low compared to the experimental data, and this is attributed to the turbulent flow prevailing there. Yet, the capability of the method to yield prediction in the separated regions has been demonstrated.

The present calculations can be used to study the conditions and symptoms of separation. Further analysis of the data in the whole flow field by appropriate visualization of the numerical solution is needed to obtain final conclusions. It should be noted that complete simulations of three-dimensional separated flow fields require turbulent flow modelling as well, since separated regions are usually turbulent. Also, the boundary conditions at the upstream boundary must be improved, perhaps by solving the flow field from the forward stagnation point. These studies are currently under way and will be reported in due course.

Acknowledgement

The research was partially supported by Stiftung Volkswagenwerk Grant No. I/37270.

References

1. Peake, D.J. and Tobak, M., "Three-Dimensional Interactions and Vortical Flow with Emphasis on High Speeds", AGARDograph 252, July 1980.
2. Maltby, R.L., "Flow Visualization in Wind Tunnels Using Indicators", AGARDograph 70, 1962.
3. Lighthill, M.J., "Attachment and Separation in Three-Dimensional Flow in Laminar Boundary Layers", Laminar Boundary Layers, Oxford Univ. Press, 1963, pp. 72-82.
4. Maskell, E.C., "Flow Separation in Three-Dimensions", RAE Aero. Report 2565, 1955.
5. Wang, K.C., "Separation Patterns of Boundary Layer Over an Inclined Body of Revolution", AIAA Journal, Vol. 10, August 1972, pp. 1044-1050.
6. Han, T.Y. and Patel, V.C., "Flow Separation on a Spheroid at Incidence", Journal of Fluid Mechanics, Vol. 92, 1979, pp. 643-657.
7. Kreplin, H.P., Vollmers, H. and Meier, H.U., "Measurements of the Wall Shear Stress on an Inclined Prolate Spheroid", Zeitschrift fur Flugwissenschaft Weltraumforschung, Vol. 6, 1982, pp. 248-252.
8. Wang, K.C., "Three-Dimensional Boundary Layer Near the Plane of Symmetry of a Spheroid at Incidence", Journal of Fluid Mechanics, Vol. 43, 1970, pp. 187-209.
9. Wang, K.C., "Boundary Layer Over a Blunt Body at Low Incidence with Circumferential Reversed Flow", Journal of Fluid Mechanics, Vol. 72, 1975, pp. 49-65.
10. Cebeci, T., Khattab, A.A. and Stewartson, K., "Three-Dimensional Laminar Boundary Layers and the Ok of Accessibility", Journal of Fluid Mechanics, Vol. 107, 1981, pp. 57-87

11. Hirsch, R.S. and Cebeci, T., "Calculation of Three-Dimensional Boundary Layers with Negative Cross Flow on Bodies of Revolution", AIAA Paper 77-683, 1977.
12. Patel, V.C. and Choi, D.H., "Calculation of Three-Dimensional Laminar and Turbulent Boundary Layers on Bodies of Revolution at Incidence", Turbulent Shear Flows II, edited by L.J.S. Bradbury, F. Durst, B.E. Launder, F.W. Schmidt and J.H. Whitelaw, Springer-Verlag, New York, 1980, pp. 199-217.
13. Schoenauer, W., private communication, 1984.
14. Patel, V.C. and Baek, J.H., "Boundary Layers and Separation on a Spheroid at Incidence", AIAA Journal, Vol. 23, January 1985, pp. 55-63.
15. Stock, H.W., "Laminar Boundary Layers on Inclined Ellipsoids of Revolution", Zeitschrift fur Flugwissenschaft Weltraumforschung, Vol. 4, 1980, pp. 217-224.
16. Hung, C.M., "Numerical Solution of Supersonic Laminar Flow Over an Inclined Body of Revolution", AIAA Journal, Vol. 18, 1980, pp. 921-928.
17. Haase, W., "Separation and Vortex Pattern on a Spheroid at Incidence", Proceedings of 5th USAF/FRG Data Exchange Agreement Meeting, AFFDL-TR-80-3088, 1980, pp. 287-305.
18. Rosenfeld, M. and Israeli, M., "Numerical Solution of Incompressible Flows by a Marching Multi-Grid Nonlinear Method", AIAA Paper 85-1500, 1985.
19. Rosenfeld, M., "Numerical Solution of Viscous Incompressible Flow Around a Slender Body at Incidence", Ph.D. Thesis, Department of Aeronautical Engineering, Technion, Haifa, Israel, 1986.

List of Figures

Fig. 1: The coordinate system.

Fig. 2: The distribution of the normalized skin friction coefficient on the symmetry planes of the 4:1 spheroid at 6° incidence.

Fig. 3: Comparison of the skin friction components with the results of Patel and Choi¹² for the 4:1 spheroid at 6° incidence.

Fig. 4: Skin friction vector plot for the unwrapped 4:1 spheroid at 6° incidence.

Fig. 5a: Skin friction lines on the unwrapped 4:1 spheroid at 6° incidence.

Fig. 5b: Skin friction lines on the 4:1 spheroid at 6° incidence.

Fig. 6: Comparisons of the separation and of the zero circumferential shear stress lines with other results for the 4:1 spheroid at 6° incidence.

Fig. 7: Comparison of the absolute magnitude of the normalized skin friction coefficient with other results for the 6:1 spheroid at 10° incidence.

Fig. 8: Skin friction vector plot for the unwrapped 6:1 spheroid at 10° incidence.

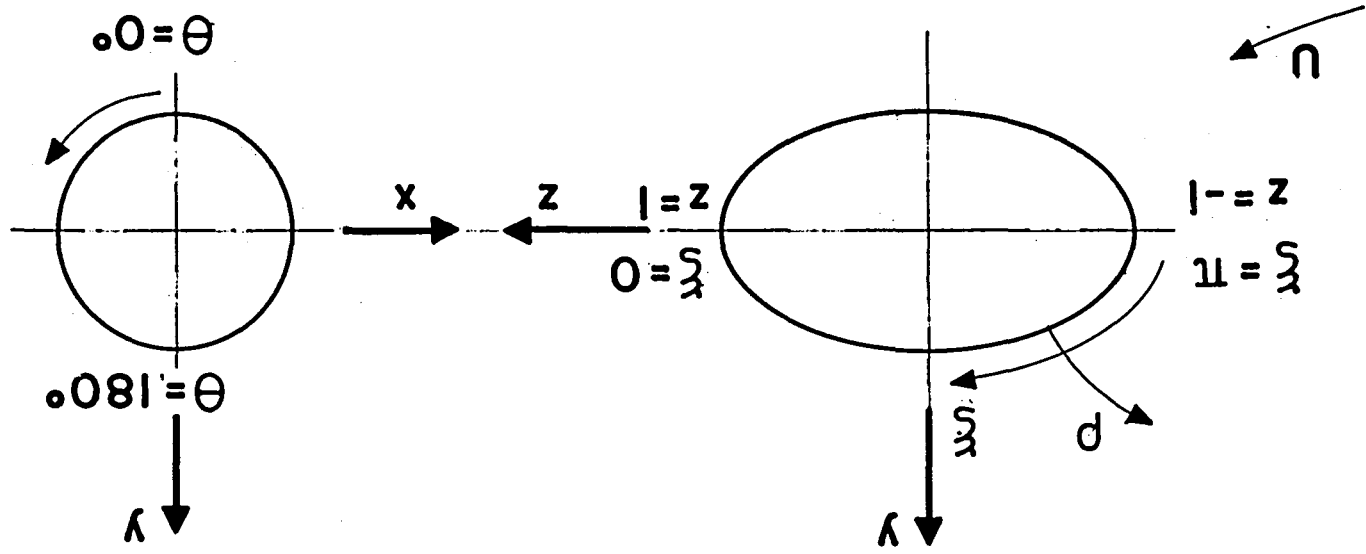
Fig. 9a: Computed skin friction coefficient compared to Kreplin et al. experiments⁷.

Fig. 9b: Computed skin friction coefficient compared to boundary layer results of Schoenauer¹³.

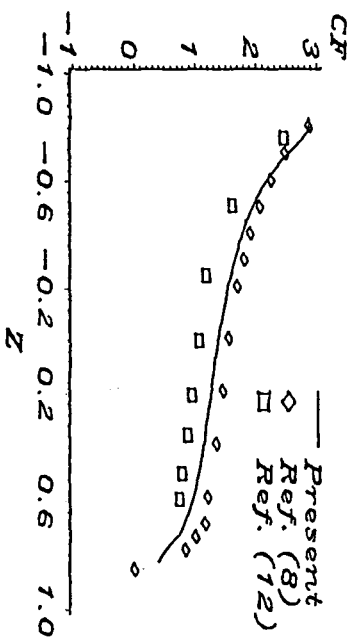
Fig. 10a: Skin friction lines on the unwrapped 6:1 spheroid at 10° incidence.

Fig. 10b: Skin friction lines on the 6:1 spheroid at 10° incidence.

Fig. 1



(a)
WINDWARD



(b)
LEEWARD

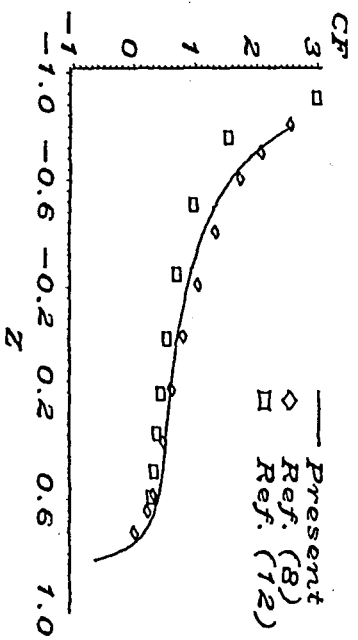
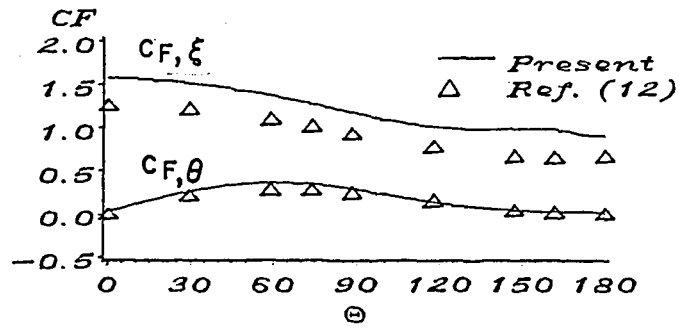


Fig. 2

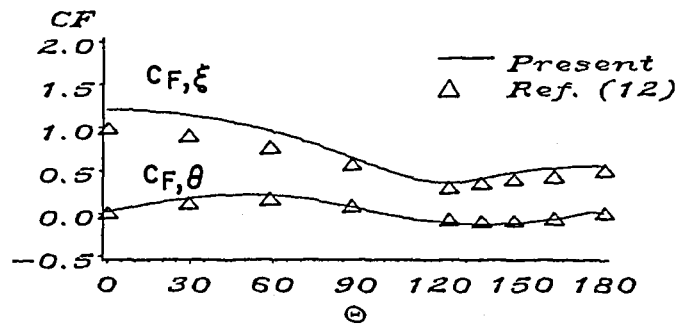
(a)

$Z = -0.250$



(b)

$Z = 0.250$



(c)

$Z = 0.600$

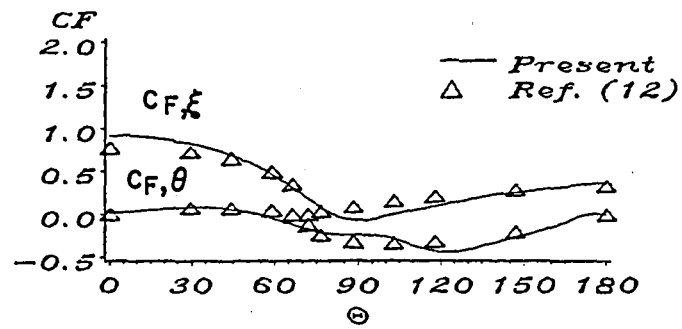


Fig. 3

SPHEROID 4:1, 6 DEG.

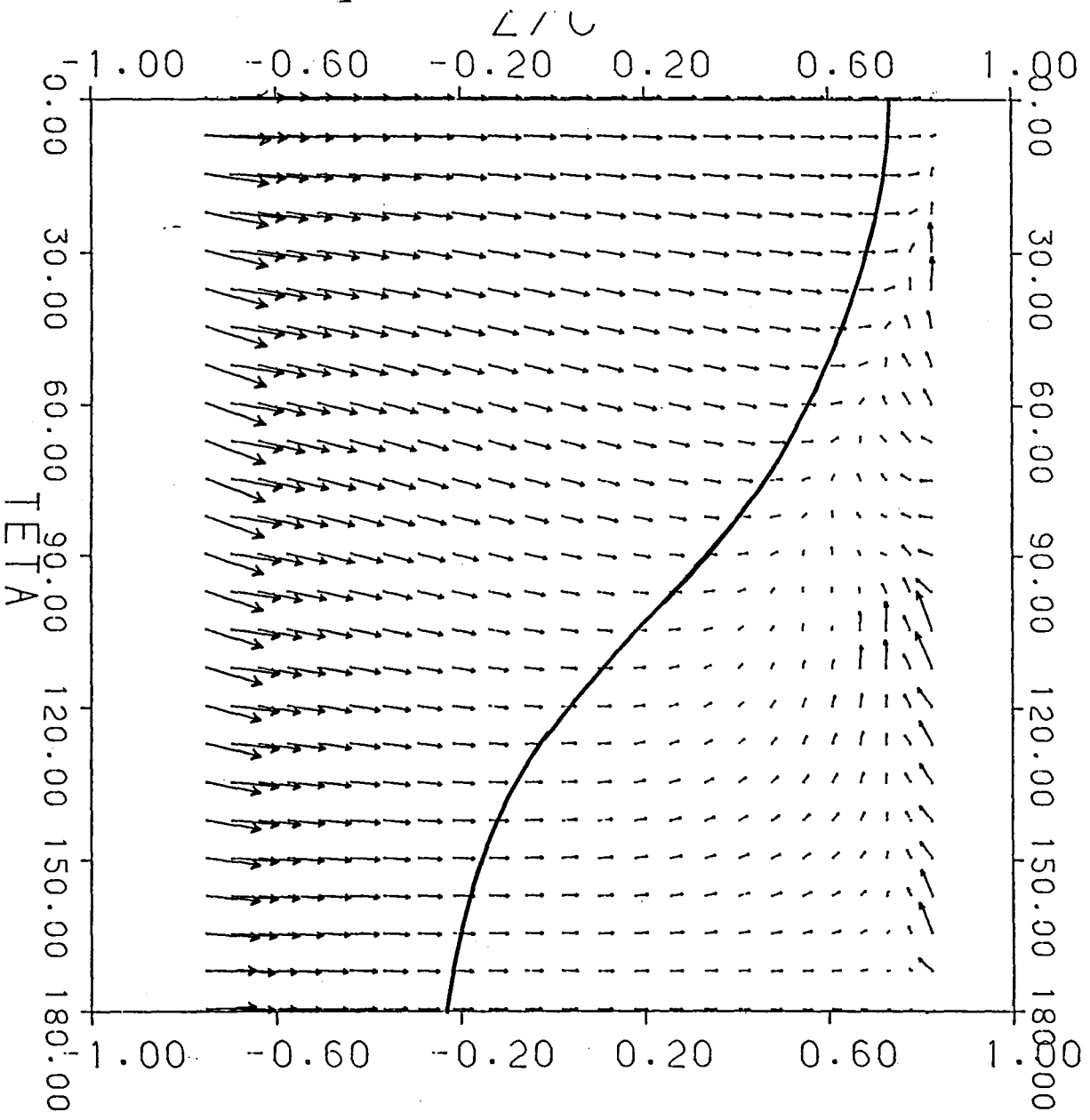


Fig. 4

SPHEROID 4:1, 6 DEG.

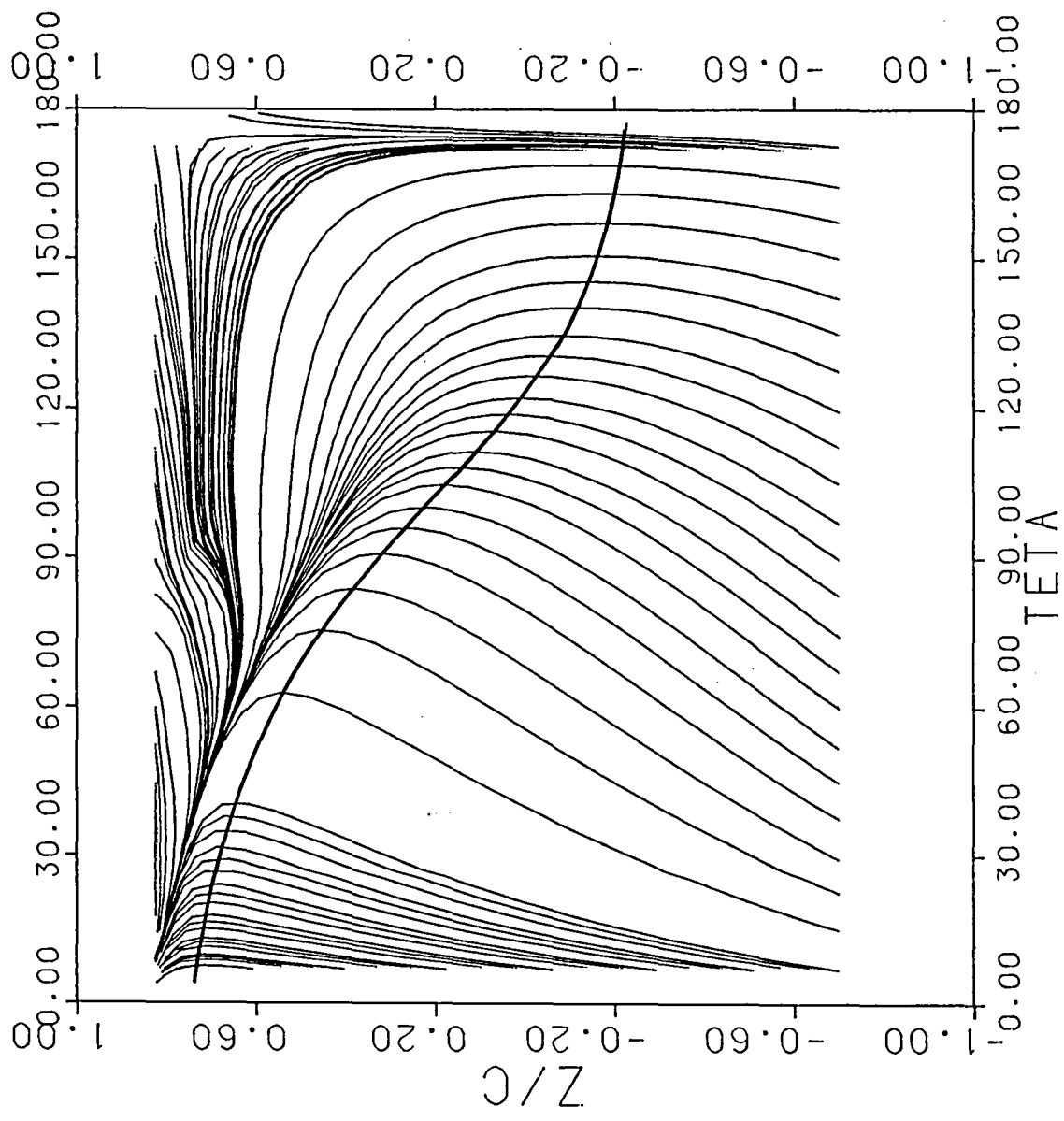
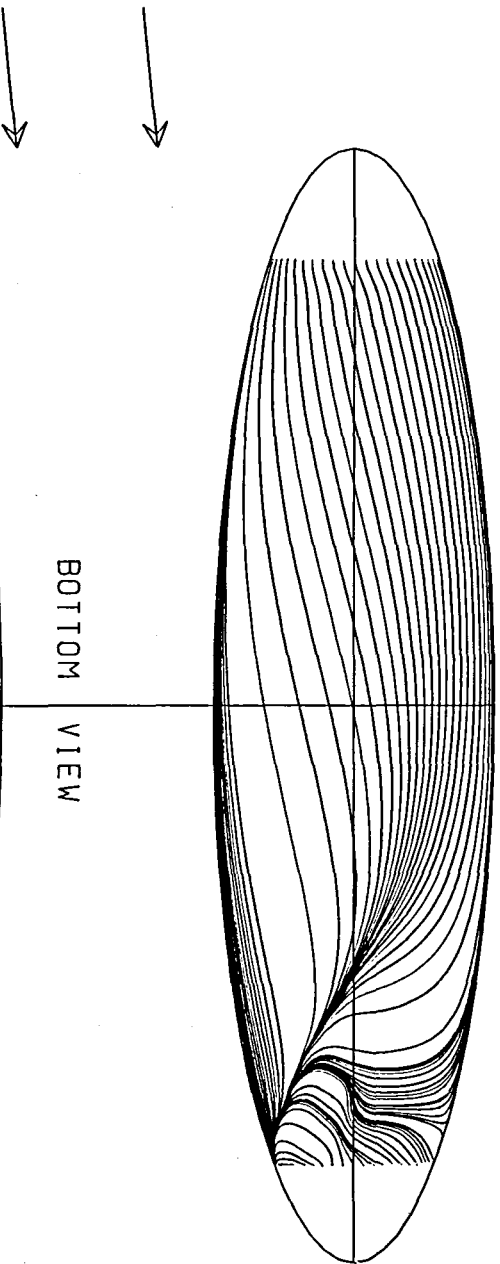


Fig. 5a

SPHEROID 4:1, 6 DEG.

SIDE VIEW



BOTTOM VIEW

TOP VIEW

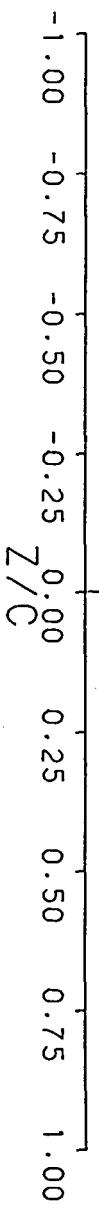


Fig. 5b

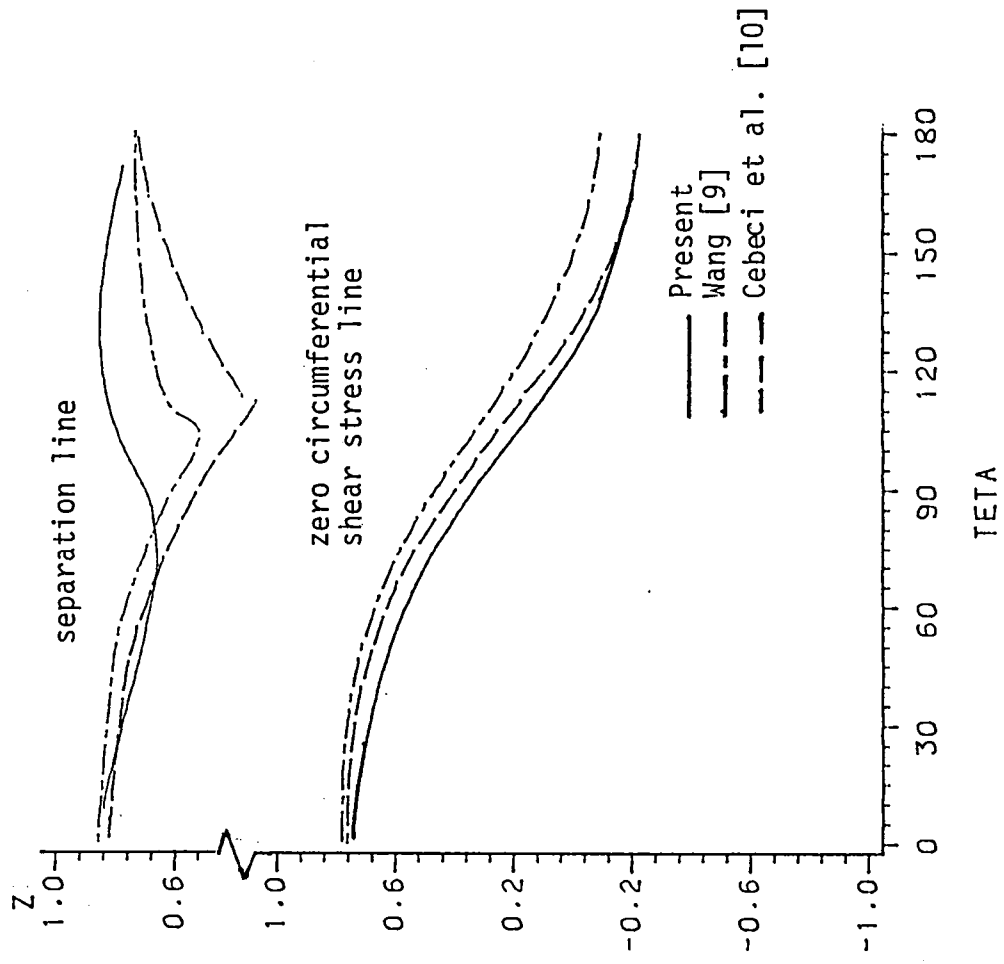
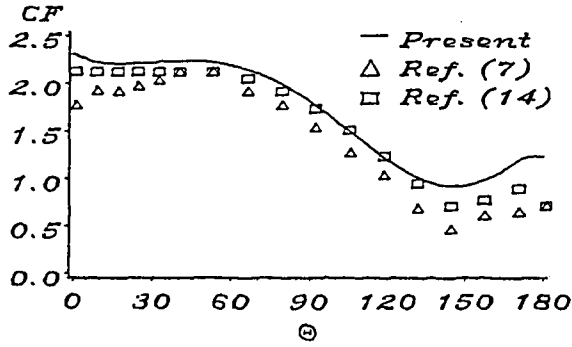


Fig. 6

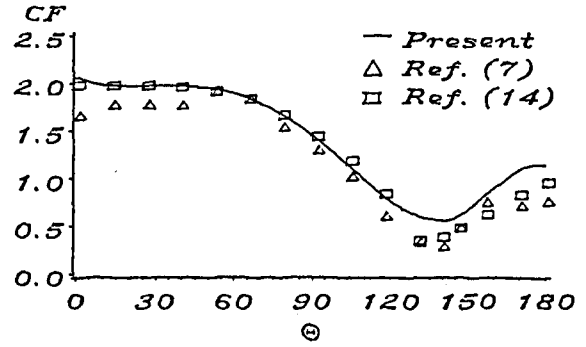
(a)

$Z = -0.554$



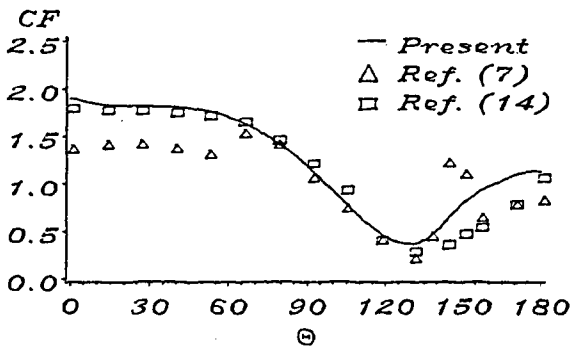
(b)

$Z = -0.382$



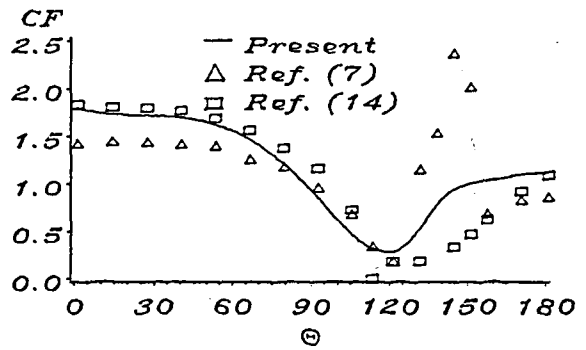
(c)

$Z = -0.210$



(d)

$Z = -0.038$



(e)

$Z = 0.134$

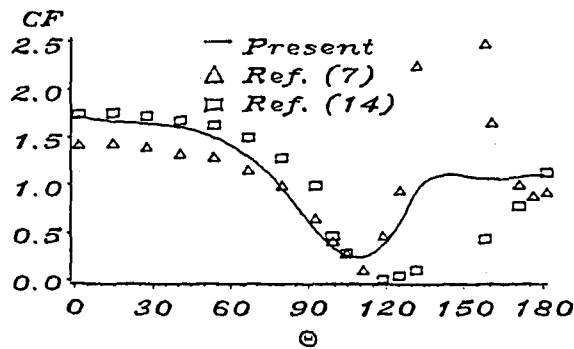


Fig. 7

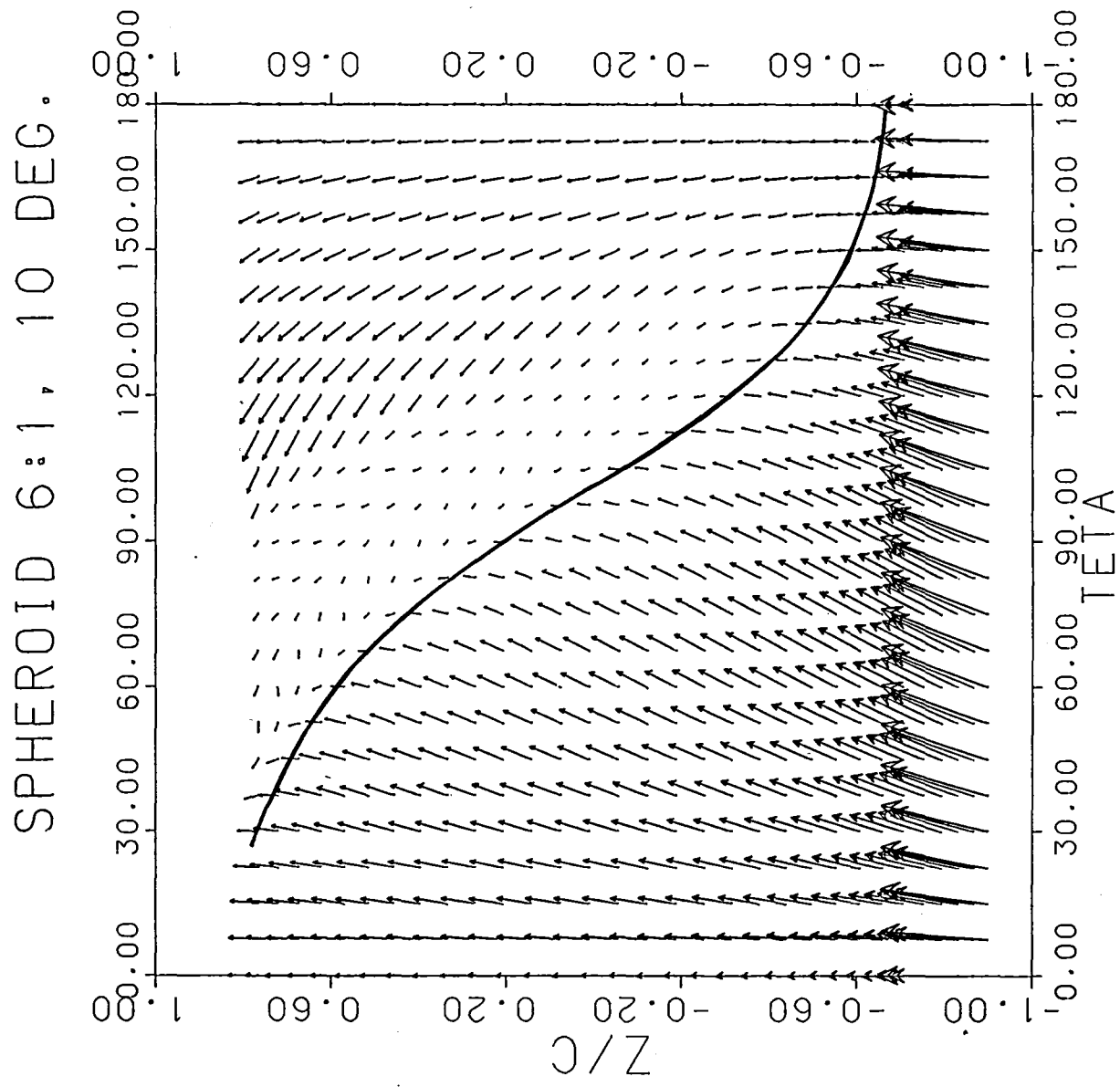


Fig. 8

SPHEROID 6:1, 10 DEG.

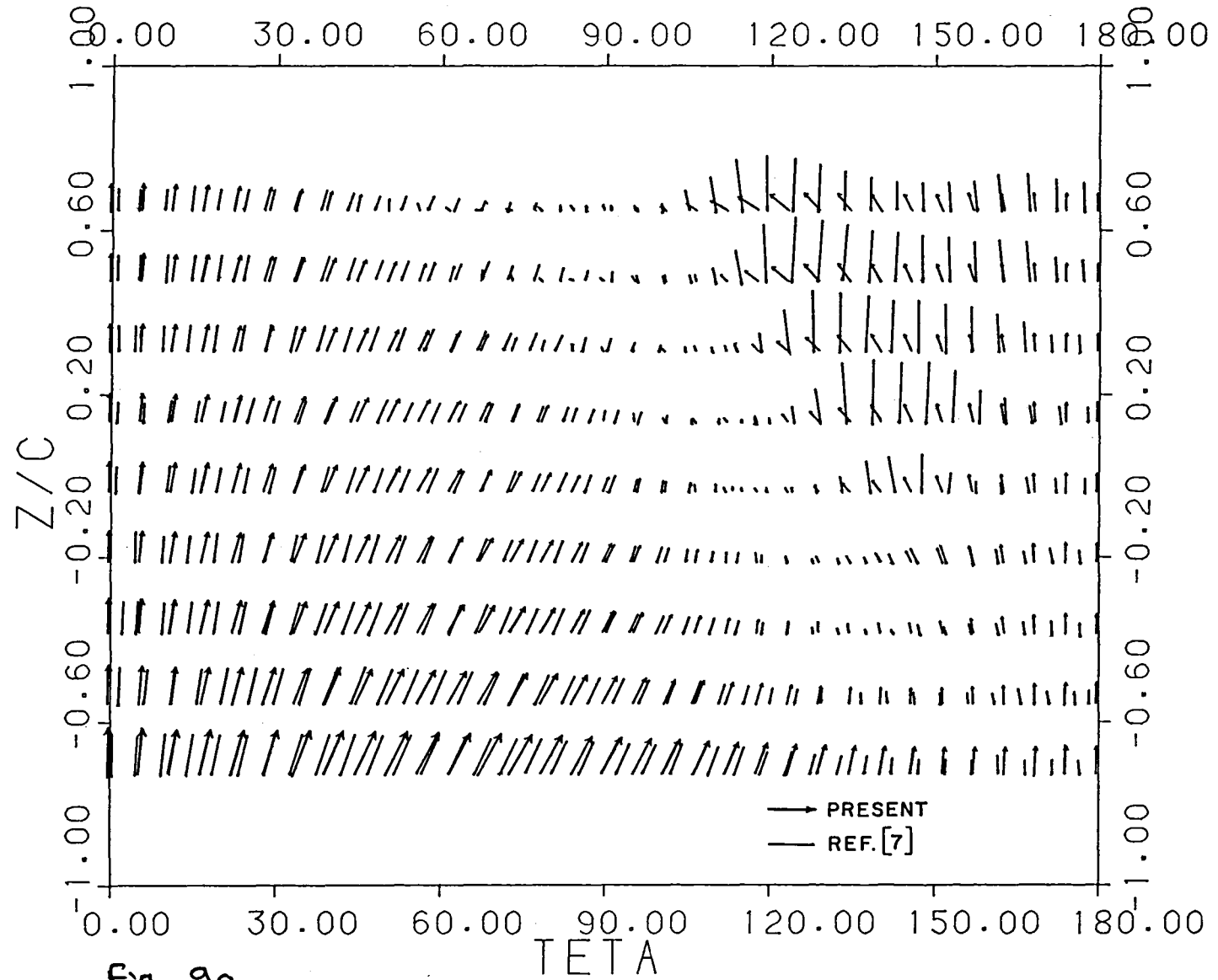
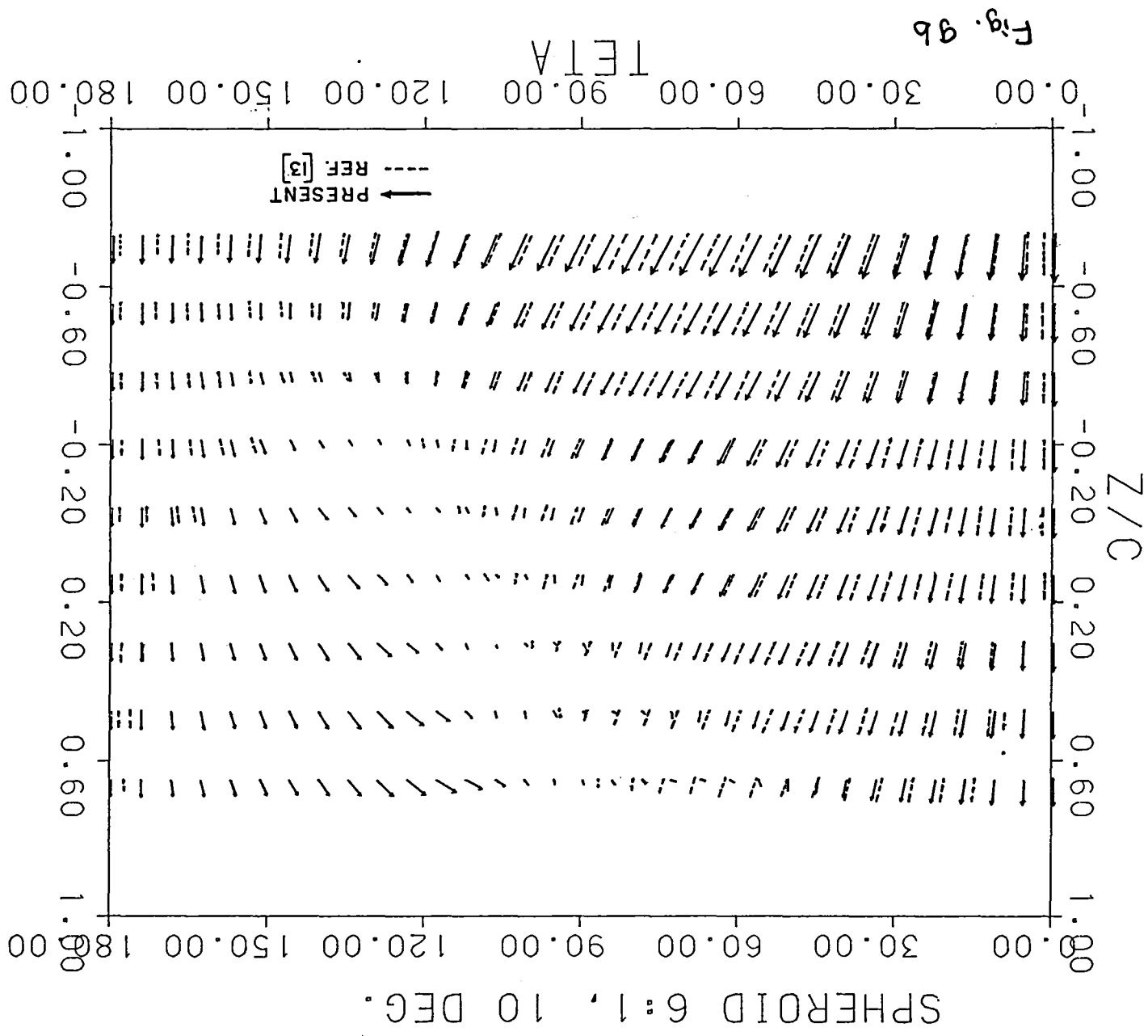


Fig. 9a



SPHEROID 6:1, 10 DEG.

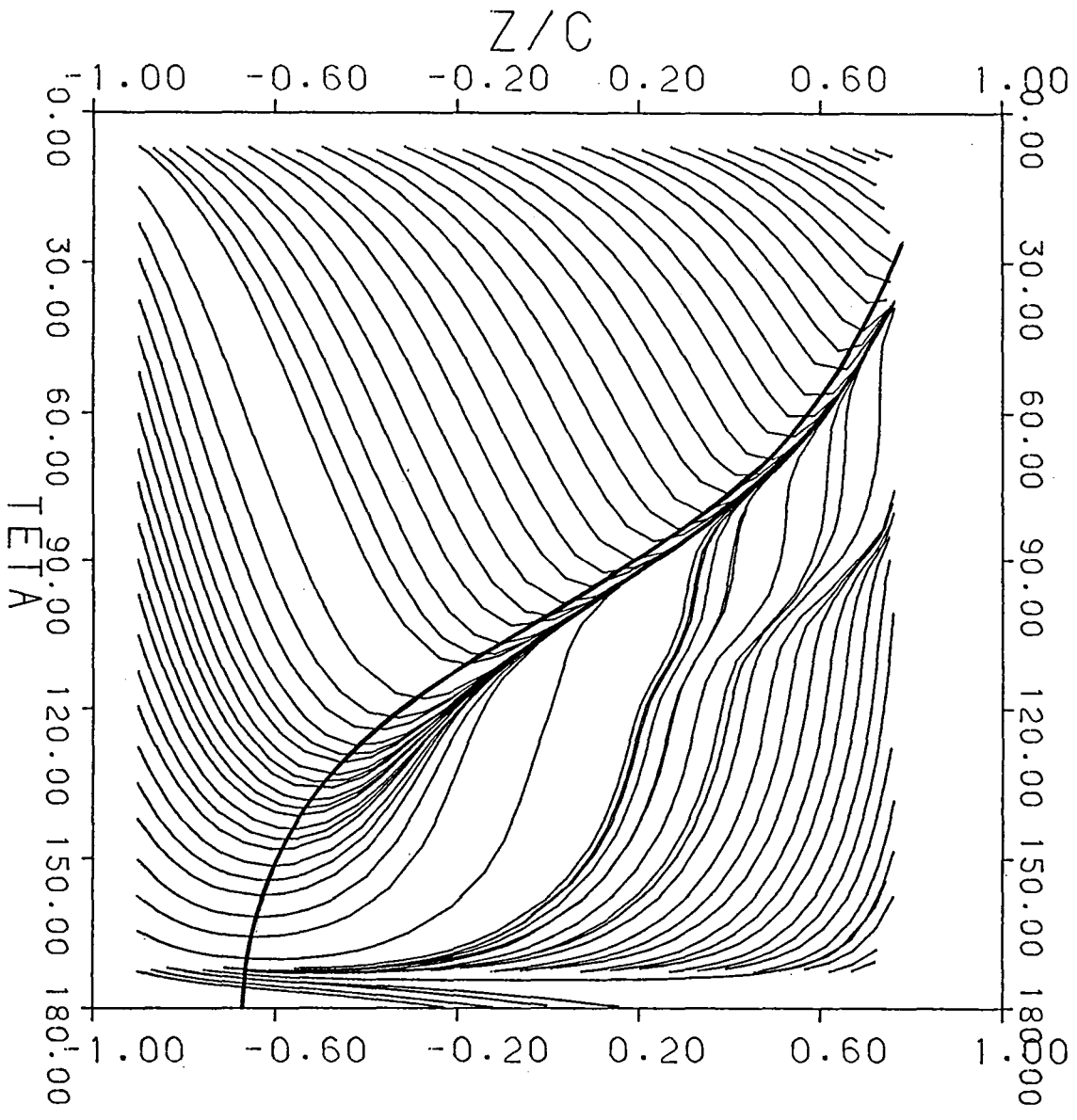
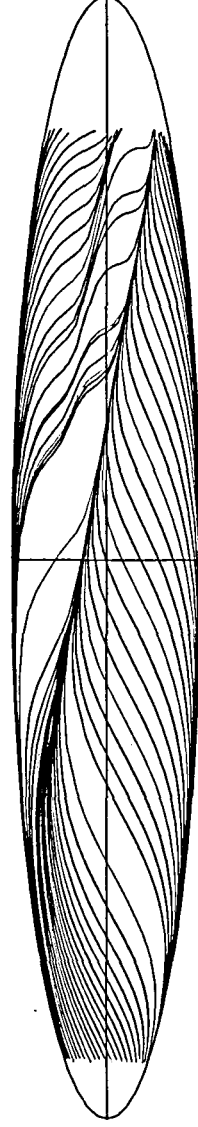


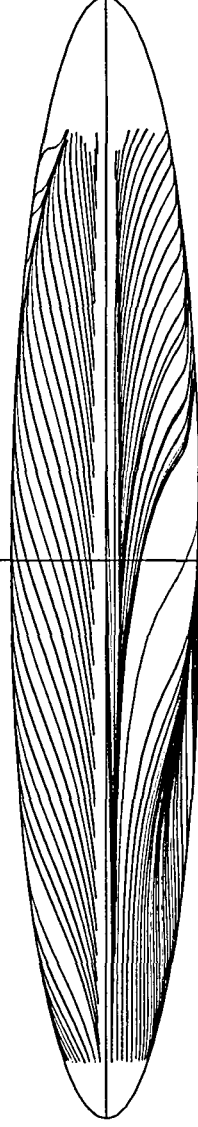
Fig. 10a

SPHEROID 6:1, 10 DEG.

SIDE VIEW



BOTTOM VIEW



TOP VIEW

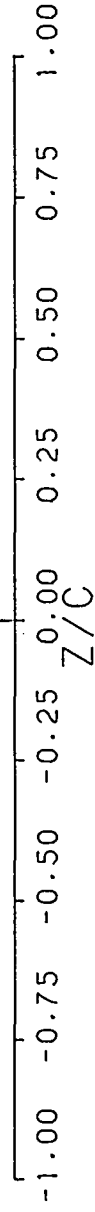


Fig. 10b

Standard Bibliographic Page

1. Report No. NASA CR-178167 ICASE Report No. 86-49		2. Government Accession No.		3. Recipient's Catalog No.	
4. Title and Subtitle A NUMERICAL STUDY OF SEPARATION ON A SPHEROID AT INCIDENCE				5. Report Date July 1986	
				6. Performing Organization Code	
7. Author(s) M. Rosenfeld, M. Israeli, and M. Wolfshtein				8. Performing Organization Report No. 86-49	
				10. Work Unit No.	
9. Performing Organization Name and Address Institute for Computer Applications in Science and Engineering Mail Stop 132C, NASA Langley Research Center Hampton, VA 23665-5225				11. Contract or Grant No. NAS1-17070, NAS1-18107	
				13. Type of Report and Period Covered Contractor Report	
12. Sponsoring Agency Name and Address National Aeronautics and Space Administration Washington, D.C. 20546				14. Sponsoring Agency Code 505-31-83-01	
15. Supplementary Notes Langley Technical Monitor: Submitted to AIAA J. C. South Final Report					
16. Abstract The three-dimensional incompressible, steady and laminar flow field around a prolate spheroid at incidence is considered. The parabolized Navier-Stokes equations are solved numerically. The method can handle vortex type as well as bubble type flow separation because the pressure is one of the dependent variables. In the present paper the distribution of the skin friction is reported for two test cases. The first test case is a prolate spheroid of aspect ratio of 4:1 at 6° incidence and Reynolds number of 10 ⁶ (based on half the major axis). The second case is a spheroid with a 6:1 aspect ratio at 10° incidence and Reynolds number of 0.8·10 ⁶ . The properties of the flow field near the body are discussed on the basis of the pattern of the skin friction lines, and the shape of the separation lines. Favorable agreement with experimental results is obtained.					
17. Key Words (Suggested by Authors(s)) laminar flow, parabolized Navier-Stokes, separation			18. Distribution Statement 34 - Fluid Mechanics and Heat 64 - Numerical Analysis Unclassified - unlimited		
19. Security Classif. (of this report) Unclassified		20. Security Classif. (of this page) Unclassified		21. No. of Pages 35	
				22. Price A03	

For sale by the National Technical Information Service, Springfield, Virginia 22161

End of Document